Near-infrared spectral monitoring of Triton with IRTF/SpeX I: Establishing a baseline for rotational variability

W.M. Grundy[1]
Lowell Observatory, 1400 W. Mars Hill Rd., Flagstaff AZ 86001
W.Grundy@lowell.edu

L.A. Young[1]
Southwest Research Institute, 1050 Walnut St., Boulder CO 80302
layoung@boulder.swri.edu

[1]Visiting observer at the Infrared Telescope Facility, which is operated by the University of Hawaii under contract from the National Aeronautics and Space Administration

— Submitted to *Icarus* —

Received 2004/04/07 ; accepted _____

Primary contact:	Will Grundy
E-mail:	*W.Grundy@lowell.edu*
Voice:	928-774-3358
Fax:	928-774-6296

Running head:	Triton monitoring
Manuscript pages:	37
Figures:	10
Tables:	1

ABSTRACT

We present eight new 0.8 to 2.4 μm spectral observations of Neptune's satellite Triton, obtained at IRTF/SpeX during 2002 July 15–22 UT. Our objective was to determine how Triton's near-infrared spectrum varies as Triton rotates, and to establish an accurate baseline for comparison with past and future observations. The most striking spectral change detected was in Triton's nitrogen ice absorption band at 2.15 μm; its strength varies by about a factor of two as Triton rotates. Maximum N_2 absorption approximately coincides with Triton's Neptune-facing hemisphere, which is also the longitude where the polar cap extends nearest Triton's equator. More subtle rotational variations are reported for Triton's CH_4 and H_2O ice absorption bands. Unlike the other ices, Triton's CO_2 ice absorption bands remain nearly constant as Triton rotates. Triton's H_2O ice is shown to be crystalline, rather than amorphous. Triton's N_2 ice is confirmed to be the warmer, hexagonal, β N_2 phase, and its CH_4 is confirmed to be highly diluted in N_2 ice.

Subject headings: Ices; satellite surfaces; satellites of Neptune; infrared observations; volatile transport

1. Introduction

Neptune's moon, Triton, experiences complex seasonal variations in its subsolar latitude due to the combination of Neptune's obliquity and Triton's inclined orbit (Trafton 1984; Forget *et al.* 2000). These variations are expected to drive complex seasonal changes in Triton's surface and atmosphere. Because Triton's N_2-dominated atmosphere is in vapor-pressure equilibrium with its N_2 surface ice, small changes in ice temperature cause extreme changes in surface pressure (Brown and Ziegler 1980). As changes in subsolar

latitude alter insolation patterns, Triton's surface pressure is expected to vary by one to two orders of magnitude (Trafton 1984; Stansberry *et al.* 1990; Hansen and Paige 1992; Spencer and Moore 1992; Forget *et al.* 2000), with corresponding seasonal changes in the distributions of volatile N_2, CO, and CH_4 ices on Triton's surface.

Observers have reported evidence of change on Triton on both long and short time scales, from stellar occultations, and from spectroscopy and photometry at UV, visible, and IR wavelengths. Stellar occultations in 1993, 1995, and 1997 indicate that Triton's atmospheric pressure has increased since the 1989 Voyager encounter, with the surface pressure rising from 14 to 19 μbar (Elliot *et al.* 1998, 2000a,b). Visible photometry spanning 1952 to 1990 shows a long-term blue-ing trend in Triton's $U-B$ and $B-V$ colors (Buratti *et al.* 1994). Superimposed on this trend are occasional reddening episodes with time scales of less than a year (Buratti *et al.* 1999; Hicks and Buratti 2004); a similar reddening was also seen between 1977 and 1989 (see Brown *et al.* 1995, for a review). These reddenings decrease the flux at 0.35 μm by nearly a factor of two relative to the flux at 0.6 μm. In the mid-UV (0.279-0.311 μm) Triton brightened by roughly 27% between 1993 and 1999 (Young and Stern 2001). These interannual changes in UV and visible albedos and colors are much larger than variations seen with rotational phase; Triton's lightcurve amplitude at 0.27 μm is 8%, and only 5% at 0.35 μm (Hillier *et al.* 1991; Young and Stern 2001), so the observed changes reflect secular, rather than rotational variations. Similarly, the occultation results most likely imply global-scale changes (Elliot *et al.* 2000b).

Interpretations of these changes have invoked effects including volatile transport (e.g., Trafton 1984; Spencer 1990; Stansberry *et al.* 1990; Hansen and Paige 1992; Grundy and Stansberry 2000), photochemical processing of atmospheric gases and surface ices (e.g., Delitsky and Thompson 1987; Johnson 1989; McDonald *et al.* 1994; Salama 1998; Strazzulla 1998; Hudson and Moore 2001; Moore and Hudson 2003), changes in ice particle

size and porosity due to annealing or sintering (e.g., Clark *et al.* 1983; Eluszkiewicz 1991; Eluszkiewicz *et al.* 1998; Eluszkiewicz and Moncet 2003), and atmospheric deposition, mechanical under-turning, and thermally-induced submersion, of thin (∼100 micron) layers on Triton's surface (as discussed by Young and Stern 2001).

To test the theoretical models and to make sense of the clues from occultation, UV, and visible data, we want to monitor changes in the composition, mixing state, temperature, and grain sizes of the ices on Triton's surface. To date, the near-infrared is the only spectral region to reveal this information (e.g., Cruikshank *et al.* 1993; Quirico *et al.* 1999; Cruikshank *et al.* 2000). Historical evidence for spectral changes at near-infrared wavelengths is ambiguous. As reviewed by Brown *et al.* (1995), Triton's CH_4 absorption bands were stronger in 1980 (on Triton's leading hemisphere) than in 1981 (on Triton's trailing hemisphere). It is unclear whether these changes are related to spatial or temporal variability. Furthermore, the earlier datasets have very low signal-to-noise and spectral resolution ($\lambda/\Delta\lambda$ ∼20 in 1980) compared with what can be routinely obtained at present.

To improve temporal sampling of Triton's near-infrared spectrum, in 2002 we began a new program of high-quality spectroscopic monitoring using consistent data acquisition methods, with observations roughly once a month during each Triton apparition. In light of possible longitudinal variation in CH_4 band strength (e.g., Cruikshank and Apt 1984; Cruikshank *et al.* 1988), we began this program by observing Triton on eight consecutive nights. These initial observations, the subject of this paper, serve two purposes. First, being spaced at roughly 61° subsolar longitude intervals, these observations provide information on the longitudinal distribution of ices on Triton's surface. Second, they create a fiducial data set against which to compare past and future observations by ourselves and others.

2. Observations and Reduction

We obtained rotationally resolved infrared spectroscopy of Triton over eight consecutive nights (2002 July 15–22 UT) at NASA's Infrared Telescope Facility (IRTF) on Mauna Kea as tabulated in Table 1. Triton's rotational period and orbital period about Neptune are both 5.877 days, so 8 nights provided some protection against weather loss and also enabled direct comparison of similar rotational phases at the beginning and end of our run. Weather was acceptable for spectroscopy on all eight nights. We used the short cross-dispersed mode of the SpeX spectrograph (Rayner *et al.* 1998, 2003), covering the 0.8 to 2.4 μm wavelength range with five spectral orders, recorded simultaneously on a 1024×1024 InSb array.

EDITOR: Please place TABLE 1 near here.

To minimize spurious spectral slopes which can arise from differential atmospheric refraction, we used an image rotator to keep SpeX's 0.3 arcsec slit oriented on the sky-plane as close to the parallactic angle as possible. The parallactic angle is the sky-plane projection of the plane defined by observer-object and observer-zenith vectors, and gives the orientation on the sky-plane of light dispersion due to differential atmospheric refraction. It is desirable to maintain alignment of the slit with the parallactic angle, especially at high airmasses, but the necessity of keeping Neptune well away from the slit interfered with that goal. Near transit, when the airmass was low (∼1.3) and the parallactic angle rotated rapidly, we kept the slit within 60° of the parallactic angle. During the more critical higher airmass observations (nightly maximum airmass was ∼1.85) we kept the slit within 15° of the parallactic angle, resulting in a maximum cross-slit dispersion between 0.8 and 2.4 μm of less than 0.2 arcsec, which compares favorably with the 0.6 arcsec width of the best K band seeing disk encountered during the run. We could not find evidence in our Triton data for the spurious spectral slopes characteristic of differential refraction problems.

Spectral extraction was accomplished using the Horne (1986) optimal extraction algorithm as implemented by M.W. Buie *et al.* at Lowell Observatory (e.g., Buie and Grundy 2000; Grundy and Buie 2001; Grundy *et al.* 2002a).

We alternated observations of Triton with those of nearby reference star HD 202282, cataloged as spectral class G3V (Houk and Smith-Moore 1988), in addition to more distant, well-known solar analogs 16 Cyg B, BS 5968, BS 6060, and SA 112-1333. Observations of the latter four stars were used to determine that HD 202282 is also an excellent solar analog in this spectral range. From the suite of solar analog observations obtained each night we computed telluric extinction, enabling us to correct all star and Triton observations to a common airmass. We then divided the airmass-corrected Triton spectra by the mean of the airmass-corrected solar analog spectra. Because the flux from Triton is entirely due to reflected sunlight over the observed wavelength range, this operation produced spectra proportional to Triton's disk-integrated albedo, as well as eliminating most instrumental and telluric spectral features. Residual telluric features do remain near 1.4 and 1.9 μm, where strong and narrow telluric H_2O vapor absorptions make sky transparency especially variable in time. Final, normalized albedo spectra of Triton from the eight nights are shown in Fig. 1.

EDITOR: Please place FIGURE 1 near here.

Wavelength calibration was derived from telluric sky emission lines extracted from the Triton frames and from separate observations of SpeX's internal integrating sphere, illuminated by a low-pressure argon arc lamp. Profiles of these line sources were well approximated by Gaussians having full width at half maximum (FWHM) of $\sim$2.5 pixels, implying resolving power ($\lambda/\Delta\lambda$) between 1600 and 1700 over our spectral range. Wavelength uncertainty, primarily due to flexure within SpeX, is approximately one pixel.

With Triton and reference star seeing disks uniformly wider than the slit, these filled slit resolutions and wavelength uncertainties apply to all of our observations.

It is not possible to quote absolute albedos from narrow-slit spectra alone, since variable slit losses (e.g., due to tracking or changes in seeing) undermine the photometric fidelity of comparisons between targets and standards. For the night of 2002 July 21, M. Connelly kindly took JHK photometry of Triton for us with the University of Hawaii's 2.2 m telescope at Mauna Kea with the QUIRC IR array (Hodapp *et al.* 1996). The standard star was FS137 (from the UKIRT extended faint standards list, Casali and Hawarden 1992), and we corrected for the ∼0.5 airmass difference using the mean Mauna Kea extinction values of Krisciunas *et al.* (1987). Under these assumptions, Triton's average geometric albedos were 0.964, 0.811, and 0.603 through the J, H, and K filters, respectively, on this night, consistent (to the 10% quality of our photometry) with the IR colors tabulated in Cox (2000).

3. Analysis and Discussion

The eight Triton spectra in Fig. 1 appear qualitatively similar to one another, but close examination reveals subtle differences. The most significant of these is a variation in the depth of the β N_2 ice absorption band at 2.15 μm, as becomes more apparent in the enlarged view in Fig. 2. This variation can be quantified by computing the integrated area of that band in each night's spectrum, as plotted versus subsolar longitude in Fig. 3. The data reveal a nearly-sinusoidal rotational variation with maximum nitrogen absorption seen when Triton's Neptune-facing hemisphere is oriented toward the observer. The sinusoidal best-fit peak-to-peak variation is 96±16%.

EDITOR: Please place FIGURE 2 near here.

EDITOR: Please place FIGURE 3 near here.

This nearly factor of two rotational variation in Triton's N_2 absorption band could result from numerous possible physical variations with longitude on Triton. For instance, as seen from Earth, a factor of two change in Triton's N_2 ice-covered projected area as Triton spins on its axis could cause a factor of two change in the observed absorption band. A longitudinal change in thickness of a nitrogen ice glaze could have a similar effect, as could a change in the density of scattering centers or absorbing particles embedded in such a glaze (e.g., Eluszkiewicz 1991; Duxbury *et al.* 1997; Eluszkiewicz and Moncet 2003). If Triton's nitrogen ice is granular, a change in its mean grain size with longitude could also produce the observed variation.

Triton's subsolar (and sub-Earth) latitude during the time of our observations was $-50°$, near the peak of a maximum southern summer (e.g., Trafton 1984; Forget *et al.* 2000). Regardless of the specific origin of the variation in N_2 mean optical path length as Triton rotates, such high sub-observer latitudes tend to suppress rotational variations because much of the observable hemisphere remains in continuous view. Only regions north of $-40°$ latitude actually rotate out of view as Triton spins, but being foreshortened by proximity to Triton's limb, these regions can only contribute modestly to the total surface area projected towards Earth. Higher southern latitude regions remain in continuous view, with their projected areas varying as Triton rotates, but their ability to produce rotational variations diminishes sharply with proximity to the pole.

EDITOR: Please place FIGURE 4 near here.

To determine if a previously identified compositional unit on Triton could produce the observed rotational variation of the N_2 band, we plotted in Fig. 4 fractional projected areas versus subsolar longitude at the epoch of our observations for the six spectral units mapped by McEwen (1990) from Voyager II clear, green, and violet filter images (see also

Flynn *et al.* 1996). These units can be divided into two general classes. Triton's south polar cap comprises units 2, 3, and 5, while units 1, 4, and 6 are located in an equatorial band. From volatile transport models, N_2 ice is expected to be currently condensing at equatorial latitudes and sublimating away from high southern latitudes (e.g., Stansberry *et al.* 1990; Hansen and Paige 1992). However, all three equatorial band units are best seen when Triton's anti-Neptune hemisphere is oriented toward Earth, opposite the observed behavior of the N_2 ice bands. These data strongly imply that McEwen's three equatorial collar components are not the regions of Triton responsible for producing the observed 2.15 μm N_2 absorption band.

Unit 5 is the only McEwen spectral unit having its minimum and maximum projected areas coinciding in longitude with the observed N_2 band minimum and maximum. This unit comprises the bulk of Triton's polar cap. However, the peak-to-peak amplitude of unit 5's projected area variation is only about 21%, far below the factor of two variation exhibited by Triton's N_2 absorption band. If N_2 ice were uniformly distributed in unit 5 (optionally including any combination of minority polar cap units 2 and 3), it could not vary as dramatically with sub-viewer longitude as is observed. If the N_2 ice responsible for Triton's N_2 band is predominantly located on the polar cap, it must not be uniformly distributed across the cap. A possible resolution is that since the time of the Voyager encounter in 1989, N_2 ice could have sublimated away from high southern latitudes of the cap. If a large, pole-centered, symmetric patch of the southern cap has lost its N_2 ice, the longitudinal variations arising from the shape of the edge of the cap would be enhanced. To reach a factor of two variation in projected area, the devolatilized region would need to extend from the southern pole to about -31° latitude.

Significant high latitude N_2 ice sublimation loss is to be expected during major summers on Triton. N_2 ice should sublimate away at rates as high as a few cm per Earth year (e.g.

Spencer 1990; Stansberry *et al.* 1990; Hansen and Paige 1992; Grundy and Stansberry 2000), so several tens of cm of N_2 ice could have disappeared from high southern latitudes between the time of the Voyager encounter (1989 August) and the present observations (2002 July). Triton's total surface inventory of N_2 ice is not known, but it is possible that southern polar regions were coated by such a thin layer of N_2 ice at the time of the Voyager encounter. Alternatively, the N_2 ice at high southern latitudes could have mechanically evolved to a state which has a much higher density of scattering centers, resulting in shorter mean optical path lengths and thus little contribution to the formation of the 2.15 μm N_2 ice band, which requires mean optical path lengths of several cm. It is also possible that N_2 ice condenses as a thin glaze, invisible at the visual wavelengths explored by Voyager (e.g., Duxbury *et al.* 1997; Eluszkiewicz and Moncet 2003). This condensation need not respect the boundaries of geological or spectral units. It would simply condense wherever thermal emission exceeds absorbed solar insolation, tending to favor higher albedo regions and (currently) more northerly latitudes (e.g., Moore and Spencer 1990; Trafton *et al.* 1998). The edge of Triton's bright polar cap which extends especially close to the equator on the Neptune-facing hemisphere could be an especially favorable site for N_2 condensation. Under this scenario, high southern latitudes could have been free of N_2 ice even at the time of the Voyager encounter.

EDITOR: Please place FIGURE 5 near here.

Additional clues can be gleaned from examination of Triton's other near-infrared spectral features as functions of subsolar longitude. More subtle rotational variations can be seen in Triton's CH_4 ice absorption bands, three of which are shown in Fig. 5. The longitudinal variation of the 0.89, 1.65, and 1.73 μm CH_4 bands have best fit sinusoidal peak-to-peak amplitudes of 65±10%, 14±1% and 23±4%, respectively. Since there is strong spectroscopic evidence that Triton's CH_4 is highly diluted in N_2 ice (e.g., Cruikshank

et al. 1993; Quirico *et al.* 1999, and also this work), it is perhaps somewhat surprising not to see more similar rotational variation patterns for Triton's CH_4 and N_2 absorption bands. This evidence for different longitudinal distributions, possibly caused by different concentrations of CH_4 in Triton's N_2 ice, demands explanation. More subtle differences in longitudinal variability of different CH_4 bands offer equally important clues, with weaker CH_4 bands (such as the one at 0.89 μm) apparently showing more pronounced variability than the stronger bands. The weaker bands require greater optical path lengths to produce observable absorption, so they are more sensitive to higher CH_4 concentrations. For Pluto, differences in longitudinal variability have also been reported between N_2 and CH_4, and between different CH_4 bands, and have been interpreted as evidence for compositionally distinct reservoirs of CH_4-bearing ice (Grundy and Buie 2001). Concentration of CH_4 in N_2 ice is likely to be related to local sublimation and condensation history, with CH_4 gradually becoming more concentrated in ice undergoing sublimation, by means of solid state distillation (e.g., Trafton *et al.* 1998; Grundy and Stansberry 2000).

EDITOR: Please place FIGURE 6 near here.

A similar plot for Triton's $\nu_1 + 2\nu_2 + \nu_3$ CO_2 ice absorption band at 2.01 μm (Fig. 6) does not reveal statistically significant rotational variation (best fit sinusoidal peak-to-peak amplitude is 8±6%). The absence of stronger rotational variation implies either a surprisingly uniform longitudinal distribution of CO_2 ice on Triton, or that the CO_2 ice tends to outcrop at high latitudes. CO_2 is non-volatile at Triton surface temperatures, so it is often thought of as a component of the bedrock or substrate (along with H_2O ice and other non-volatile materials) upon which more volatile materials move about on seasonal time scales (e.g., Cruikshank *et al.* 1993; Quirico *et al.* 1999). Its occurrence at high southern latitudes is consistent with the loss of volatile ices from high southern latitudes predicted by volatile transport models. However it has recently been suggested that CO_2

may move about on seasonal time scales as well, not by sublimation and condensation, but via aeolian transport (Grundy *et al.* 2002a). The small amplitude of observed longitudinal variation in Triton's CO_2 bands would also be consistent with widely distributed CO_2 dust.

Similar techniques could not be used to quantify the longitudinal dependence of Triton's CO ice because it has only two absorption bands in our spectra, both at inconvenient wavelengths. The 0-2 transition at 2.35 μm is flanked by strong CH_4 bands so the continuum level could not be determined accurately. The 0-3 transition at 1.58 μm is entangled with a CO_2 ice absorption band and the edge of a H_2O ice band complex.

EDITOR: Please place FIGURE 7 near here.

Water ice absorption bands are so broad they span other absorption bands, interfering with computation of their integrated areas. However, it is possible to compute ratios that are sensitive to the depths of specific H_2O ice bands. For instance, Fig. 7 shows a measure of rotational variation of the depth of Triton's 1.5 μm H_2O ice band. The case for rotational variation of this absorption band is more convincing than for the CO_2 ice band discussed earlier (35$\pm$12% peak-to-peak variation for the sinusoidal fit to the H_2O ice fractional band depth), but it is intriguing that the general trend matches that of the sinusoidal fit for CO_2 (and also agrees with a tentative report of leading-trailing asymmetry of these two ices by Marchi *et al.* 2004). For both ices, the leading hemisphere seems to show slightly stronger absorptions while the trailing hemisphere shows weaker ones. Higher quality follow-up observations are needed to investigate this line of evidence, which could potentially shed light on the relation between Triton's surface CO_2 and H_2O, both non-volatile at Triton surface temperatures, with impacts, which preferentially strike Triton's leading hemisphere (e.g., Zahnle *et al.* 2001).

To search for more subtle spectral features, we combined all eight of our spectra into a grand average spectrum. Since SpeX's internal flexure caused correspondence between wavelengths and pixels to shift slightly from night to night, we re-sampled each spectrum to a common wavelength grid before computing the grand average, resulting in a slight loss of spectral resolution. Nevertheless, the grand average spectrum shown in Fig. 8 has signal precision and spectral resolution among the highest of any Triton spectrum ever published in this wavelength range.

EDITOR: Please place FIGURE 8 near here.

We compared our grand average spectrum with other recent Triton spectra and found excellent agreement in the overall spectral shape (e.g., Quirico *et al.* 1999; Cruikshank *et al.* 2000; Forni *et al.* 2001, the Cruikshank *et al.* data being reproduced in Fig. 8). Consistent with results reported by Forni *et al.* (2001) and by Marchi *et al.* (2004), our data show no evidence for three weak absorption bands tentatively reported at 1.543, 1.683, and 1.749 μm by Quirico *et al.* (1999), ruling out narrow absorption bands at these wavelengths any deeper than 1%, 1%, and 2%, respectively.

We compared the CH_4 bands in our Triton spectrum with laboratory absorption spectra of pure CH_4 and of CH_4 diluted in β N_2 ice (Quirico and Schmitt 1997; Schmitt *et al.* 1998; Grundy *et al.* 2002b). As initally reported by Cruikshank *et al.* (1993), the wavelengths of Triton's observed CH_4 absorption bands correspond precisely with the wavelengths of CH_4 highly diluted in β N_2 ice, such that the CH_4 molecules are isolated from one another rather than forming dimers or larger clusters. No convincing evidence is seen in our Triton grand average spectrum for the existence of more concentrated CH_4, contrasting with the clear evidence for ordinary CH_4 ice in Pluto's spectrum (e.g., Douté *et al.* 1999).

EDITOR: Please place FIGURE 9 near here.

Closer examination of Triton's nitrogen absorption at 2.15 μm (Fig. 9) shows its shape to be consistent with the warmer, hexagonal β ice phase, as reported by Cruikshank *et al.* (1993). No evidence is seen for the presence of the colder, cubic α N_2 phase. However, it is not possible to rule out the existence of fine-grained α N_2; small particles lead to short mean optical path lengths, and can thus produce negligible spectral contrasts for weak absorption bands such as these.

EDITOR: Please place FIGURE 10 near here.

The existence of the temperature-sensitive absorption band at 1.65 μm is the usual way to distinguish cold crystalline H_2O ice from amorphous H_2O ice (e.g., Schmitt *et al.* 1998). A strong CH_4 absorption obscures this wavelength in Triton's spectrum, but the shape and wavelength of the broader 1.5 μm H_2O band can also be used to distinguish the phase of H_2O ice. Comparing our grand average with spectral behavior of crystalline and amorphous H_2O ice in Fig. 10, it is clear from the band's wavelength and convex-shaped bottom that Triton's water ice is predominantly crystalline. This result was tentatively reported by Cruikshank *et al.* (2000), and our new data now make this conclusion quite firm. That H_2O ice on Triton's surface should be crystalline might not have been expected, since the surface temperature is low enough for H_2O ice to remain amorphous over the age of the solar system (Jenniskens *et al.* 1998). Its crystallinity is probably indicative of warmer formation conditions for Triton's H_2O ice.

4. Conclusion

New 0.8-2.4 μm spectral observations of Neptune's major satellite Triton obtained at IRTF/SpeX on eight consecutive nights in 2002 reveal periodic variations in the strengths of absorptions bands of Triton's surface ices: N_2, CH_4, and H_2O, but not CO_2. The observed variations (or lack thereof) give an indication of how these four ice species are distributed in longitude. The most heterogeneously distributed ice is N_2, which shows twice as much absorption on Triton's Neptune-facing hemisphere as on the anti-Neptune hemisphere. Comparison with maps of Triton's spectral units made from Voyager data suggest that Triton's observed N_2 ice is concentrated on low-latitude regions of Triton's polar cap, which are predominantly located on the Neptune-facing hemisphere. Non-volatile H_2O ice seems to be slightly concentrated on Triton's leading hemisphere while Triton's CH_4 ice seems to be slightly concentrated on the trailing hemisphere. Triton's CO_2 ice shows the least longitudinal variation, suggesting that it is either very uniformly distributed or that it is confined to high latitudes. Additionally, the shape of Triton's 1.5 μm water ice band complex clearly shows that Triton's H_2O ice is crystalline, rather than amorphous in phase, and the shape of Triton's 2.15 μm N_2 ice absorption is entirely consistent with the warmer, hexagonal β N_2 crystalline phase. The wavelengths of Triton's CH_4 ice absorptions are consistent with Triton's CH_4 being highly diluted in N_2 ice, albeit with longitudinally-variable concentrations. Using this data set as a baseline, we hope to detect future evolution of Triton's near-infrared spectrum, on time scales ranging from months to years.

ACKNOWLEDGMENTS: We thank W. Golisch, D. Griep, P. Sears, S.J. Bus, J.T. Rayner, and K. Crane for assistance with the telescope and with SpeX, M.W. Buie and R.S. Bussmann for contributing to the reduction pipeline, M. Showalter for the Rings Node's on-line ephemeris services, and NASA for its support of the IRTF. Thanks also to M. Connelly for contributing infrared photometric data from the University of Hawaii 2.2 m telescope, and to J.K. Hillier and an anonymous reviewer for their constructive reviews. This work was made possible by National Science Foundation grant AST-0085614 and NASA Planetary Astronomy grant NAG5-12516 to Southwest Research Institute, and by NASA Planetary Geology and Geophysics grant NAG5-10159 to Lowell Observatory. We are also grateful to the free and open source software communities for empowering us with the tools used to complete this project, notably Linux, the GNU toolkit, TEX, FVWM, Tcl/Tk, TkRat, and MySQL.

REFERENCES

Brown, G.N. Jr., and W.T. Ziegler 1980. Vapor pressure and heats of vaporization and sublimation of liquids and solids of interest in cryogenics below 1–atm pressure. *Adv. Cryogenic Eng.* **25**, 662-670.

Brown, R.H., D.P. Cruikshank, J. Veverka, P. Helfenstein, and J. Eluszkiewicz 1995. Surface composition and photometric properties of Triton. In *Neptune and Triton*, Ed. D.P. Cruikshank, University of Arizona Press, Tucson, 991-1030.

Buie, M.W., and W.M. Grundy 2000. The distribution and physical state of H_2O on Charon. *Icarus* **148,** 324-339.

Buratti, B.J., J.D. Goguen, J. Gibson, and J. Mosher 1994. Historical photometric evidence for volatile migration on Triton. *Icarus* **110,** 303-314.

Buratti, B.J., M.D. Hicks, and R.L. Newburn Jr. 1999. Does global warming make Triton blush? *Nature* **397,** 219.

Casali, M.M., and T.G. Hawarden 1992. *The JCMT-UKIRT Newsletter* **4,** 33-35.

Clark, R.N., F.P. Fanale, and A.P. Zent 1983. Frost grain size metamorphism: Implications for remote sensing of planetary surfaces. *Icarus* **56,** 233-245.

Cox, A.N. 2000. *Allen's astrophysical quantities (4^{th} ed.)*. AIP Press; Springer, New York.

Cruikshank, D.P., and J. Apt 1984. Methane on Triton: Physical state and distribution. *Icarus* **58,** 306-311.

Cruikshank, D.P., R.H. Brown, A.T. Tokunaga, R.G. Smith, and J.R. Piscitelli 1988. Volatiles on Triton: The infrared spectral evidence, 2.0-2.5 microns. *Icarus* **74,** 413-423.

Cruikshank, D.P., T.L. Roush, T.C. Owen, T.R. Geballe, C. de Bergh, B. Schmitt, R.H. Brown, and M.J. Bartholomew 1993. Ices on the surface of Triton. *Science* **261,** 742-745.

Cruikshank, D.P., B. Schmitt, T.L. Roush, T.C. Owen, E. Quirico, T.R. Geballe, C. de Bergh, M.J. Bartholomew, C.M. Dalle Ore, S. Douté, and R. Meier 2000. Water ice on Triton. *Icarus* **147,** 309-316.

Delitsky, M.L., and W.R. Thompson 1987. Chemical processes in Triton's atmosphere and surface. *Icarus* **70,** 354-365.

Douté, S., B. Schmitt, E. Quirico, T.C. Owen, D.P. Cruikshank, C. de Bergh, T.R. Geballe, and T.L. Roush 1999. Evidence for methane segregation at the surface of Pluto. *Icarus* **142,** 421-444.

Duxbury, N.S., R.H. Brown, and V. Anicich 1997. Condensation of nitrogen: Implications for Pluto and Triton. *Icarus* **129,** 202-206.

Elliot, J.L., H.B. Hammel, L.H. Wasserman, O.G. Franz, S.W. McDonald, M.J. Person, C.B. Olkin, E.W. Dunham, J.R. Spencer, J.A. Stansberry, M.W. Buie, J.M. Pasachoff, B.A. Babcock, and T.H. McConnochie 1998. Global warming on Triton. *Nature* **393,** 765-767.

Elliot, J.L., M.J. Person, S.W. McDonald, M.W. Buie, E.W. Dunham, R.L. Millis, R.A. Nye, C.B. Olkin, L.H. Wasserman, L.A. Young, W.B. Hubbard, R. Hill, H.J. Reitsema, J.M. Pasachoff, T.H. McConnochie, B.A. Babcock, R.C. Stone, and P. Francis 2000a. The prediction and observation of the 1997 July 18 stellar occultation by Triton: More evidence for distortion and increasing pressure in Triton's atmosphere. *Icarus* **148,** 347-369.

Elliot, J.L., D.F. Strobel, X. Zhu, J.A. Stansberry, L.H. Wasserman, and O.G. Franz 2000b. The thermal structure of Triton's middle atmosphere. *Icarus* **143,** 425-428.

Eluszkiewicz, J. 1991. On the microphysical state of the surface of Triton. *J. Geophys. Res.* **96,** 19219-19229.

Eluszkiewicz, J., J. Leliwa-Kopystyński, and K.J. Kossacki 1998. Metamorphism of Solar System Ices. In *Solar System Ices*, Ed. B. Schmitt, C. de Bergh, and M. Festou, Kluwer Academic Publishers, Boston, 119-138.

Eluszkiewicz, E., and J.L. Moncet 2003. A coupled microphysical/radiative transfer model of albedo and emissivity of planetary surfaces covered by volatile ices. *Icarus* **166,** 375-384.

Flynn, B., A. Stern, B. Buratti, P. Schenk, L. Trafton, and J. Mosher 1996. The spatial distribution of UV-absorbing regions on Triton. *Planet. Space Sci.* **44,** 1039-1046.

Forni, O., S. Le Mouelic, E. Quirico, C. de Bergh, F. Marchis, B. Schmitt, S. Douté, R. Prangé, and L. d'Hendecourt 2001. Near-infrared spectral observations of Triton. *Lunar and Planetary Sci.* **XXXII,** 1275 (abstract).

Forget, F., N. Decamp, C. Le Guyader 2000. A new model for the seasonal evolution of Triton. *Bull. Am. Astron. Soc.* **32,** 1082 (abstract).

Grundy, W.M., B. Schmitt, and E. Quirico 1993. The temperature dependent spectra of α and β nitrogen ice with application to Triton. *Icarus* **105,** 254-258.

Grundy, W.M., M.W. Buie, and J.R. Spencer 2002a. Spectroscopy of Pluto and Triton at 3-4 microns: Possible evidence for wide distribution of non-volatile solids. *Astron. J.* **124,** 2273-2278.

Grundy W.M., B. Schmitt, and E. Quirico 2002b. The temperature dependent spectrum of methane ice I between 0.65 and 5 microns and opportunities for near-infrared remote thermometry. *Icarus* **155,** 486-496.

Grundy, W.M., and M.W. Buie 2001. Distribution and evolution of CH_4, N_2, and CO ices on Pluto's surface: 1995 to 1998. *Icarus* **153,** 248-263.

Grundy, W.M., and B. Schmitt 1998. The temperature-dependent near-infrared absorption spectrum of hexagonal H_2O ice. *J. Geophys. Res.* **103,** 25809-25822.

Grundy, W.M., and J.A. Stansberry 2000. Solar gardening and the seasonal evolution of nitrogen ice on Triton and Pluto. *Icarus* **148,** 340-346.

Hansen, C.J., and D.A. Paige 1992. A thermal model for the seasonal nitrogen cycle on Triton. *Icarus* **99,** 273-288.

Hapke, B. 1993. *Theory of reflectance and emittance spectroscopy.* Cambridge University Press, New York.

Hicks, M.D., and B.J. Buratti 2004. The spectral variability of Triton from 1997-2000. *Icarus*, in press.

Hillier, J., J. Veverka, and P. Helfenstein 1991. The wavelength dependence of Triton's light curve. *J. Geophys. Res.* **96,** 19211-19215.

Hodapp, K.W., J.L. Hora, D.N.B. Hall, L.L. Cowie, M. Metzger, E. Irwin, K. Vural, L.J. Kozlowski, S.A. Cabelli, C.Y. Chen, D.E. Cooper, G.L. Bostrup, R.B. Bailey, and W.E. Kleinhans 1996. The HAWAII Infrared Detector Arrays: Testing and Astronomical Characterization of Prototype and Science Grade Devices. *New Astronomy* **1,** 177-196.

Horne, K. 1986. An optimal extraction algorithm for CCD spectroscopy. *Pub. Astron. Soc. Pacific* **98,** 609-617.

Houk, N., and M. Smith-Moore 1988. *Catalogue of two-dimensional spectral types for the HD stars. Vol. 4.* Dept. of Astronomy, Univ. of Michigan, Ann Arbor MI.

Hudson, R.L., and M.H. Moore 2001. Radiation chemical alterations in solar system ices: An overview. *J. Geophys. Res.* **106,** 33275-33284.

Jenniskens, P., DF. Blake, and A. Kouchi 1998. Amorphous water ice: A solar system material. In *Solar System Ices*, Ed. B. Schmitt, C. de Bergh, and M. Festou, Kluwer Academic Publishers, Boston, 139-155.

Johnson, R.E. 1989. Effect of irradiation on the surface of Pluto. *Geophys. Res. Lett.* **16,** 1233-1236.

Krisciunas, K., W. Sinton, D. Tholen, A. Tokunaga, W. Golisch, D. Griep, C. Kaminski, C. Impey, and C. Christian 1987. Atmospheric Extinction and Night-Sky Brightness at Mauna Kea. *Publ. Astron. Soc. Pacific* **99,** 887-894.

Marchi, S., C. Barbieri, M. Lazzarin, T.C. Owen, and E.M. Corsini 2004. A 0.4–2.5 μm spectroscopic investigation of Triton's two faces. *Icarus* **168,** 367-373.

McDonald, G.D., W.R. Thompson, M. Heinrich, B.N. Khare, and C. Sagan 1994. Chemical investigation of Titan and Triton tholins. *Icarus* **108,** 137-145.

McEwen, A.S. 1990. Global color and albedo variations on Triton. *Geophys. Res. Lett.* **17,** 1765-1768.

Moore, J.M., and J.R. Spencer 1990. Koyaanismuuyaw: The hypothesis of a perennially dichotomous Triton. *Geophys. Res. Lett.* **17,** 1757-1760.

Moore, M.H., and R.L. Hudson 2003. Infrared study of ion-irradiated N_2-dominated ices relevant to Triton and Pluto: Formation of HCN and HNC. *Icarus* **161,** 486-500.

Quirico, E., and B. Schmitt 1997. Near-infrared spectroscopy of simple hydrocarbons and carbon oxides diluted in solid N_2 and as pure ices: Implications for Triton and Pluto. *Icarus* **127,** 354-378.

Quirico, E., S. Douté, B. Schmitt, C. de Bergh, D.P. Cruikshank, T.C. Owen, T.R. Geballe, and T.L. Roush 1999. Composition, physical state, and distribution of ices at the surface of Triton. *Icarus* **139,** 159-178.

Rayner, J.T., D.W. Toomey, P.M. Onaka, A.J. Denault, W.E. Stahlberger, D.Y. Watanabe, and S.I. Wang 1998. SpeX: A medium-resolution IR spectrograph for IRTF. *Proc. SPIE* **3354,** 468-479.

Rayner, J.T., D.W. Toomey, P.M. Onaka, A.J. Denault, W.E. Stahlberger, W.D. Vacca, M.C. Cushing, and S. Wang 2003. SpeX: A medium-resolution 0.8–5.5 micron spectrograph and imager for the NASA Infrared Telescope Facility. *Publ. Astron. Soc. Pacific* **115,** 362-382.

Salama, F., 1998. UV photochemistry of ices. In *Solar System Ices*, Ed. B. Schmitt, C. de Bergh, and M. Festou, Kluwer Academic Publishers, Boston, 259-279.

Schmitt, B., E. Quirico, F. Trotta, and W.M. Grundy 1998. Optical properties of ices from UV to infrared. In *Solar System Ices*, Ed. B. Schmitt, C. de Bergh, and M. Festou, Kluwer Academic Publishers, Boston, 199-240.

Spencer, J.R. 1990. Nitrogen frost migration on Triton: A historical model. *Geophys. Res. Lett.* **17,** 1769-1772.

Spencer, J.R., and J.M. Moore 1992. The influence of thermal inertia on temperatures and frost stability on Triton. *Icarus* **99,** 261-272.

Stansberry, J.A., J.I. Lunine, C.C. Porco, and A.S. McEwen 1990. Zonally averaged thermal balance and stability models for nitrogen polar caps on Triton. *Geophys. Res. Lett.* **17,** 1773-1776.

Strazzulla, G., 1998. Chemistry of ice induced by bombardment with energetic charged particles. In *Solar System Ices*, Ed. B. Schmitt, C. de Bergh, and M. Festou, Kluwer Academic Publishers, Boston, 281-301.

Trafton, L. 1984. Large seasonal variations in Triton's atmosphere. *Icarus* **58,** 312-324.

Trafton, L.M., D.L. Matson, and J.A. Stansberry 1998. Surface/atmosphere interactions and volatile transport (Triton, Pluto, and Io). In *Solar System Ices*, Ed. B. Schmitt, C. de Bergh, and M. Festou, Kluwer Academic, Boston, 773-812.

Young, L.A., and S.A. Stern 2001. Ultraviolet observations of Triton in 1999 with the space telescope imaging spectrograph: 2150-3180 Å spectroscopy and disk-integrated photometry. *Astron. J.* **122,** 449-456.

Zahnle, K., P. Schenk, S. Sobieszczyk, L. Dones, and H.F. Levison 2001. Differential cratering of synchronously rotating satellites by ecliptic comets. *Icarus* **153,** 111-129.

Table 1. Circumstances of observations

UT date of observation mid-time	Transparency and K band seeing conditions	Subsolar longitude (°)	Phase angle (°)	Total integration (min)
2002/07/15.39	Clear, 1.0″	359.8	0.58	52
2002/07/16.39	Scattered clouds, 0.8″	61.1	0.55	52
2002/07/17.41	Cirrus, 0.7″	123.6	0.52	84
2002/07/18.40	Thin high clouds, 1.2″	184.1	0.49	64
2002/07/19.40	Some thin cirrus, 0.8″	245.2	0.46	68
2002/07/20.39	Some thin cirrus, 0.7″	306.3	0.42	68
2002/07/21.40	Some thin cirrus, 0.6″	7.6	0.39	68
2002/07/22.39	Very clear, 0.8″	68.5	0.36	84

FIGURE CAPTIONS

Fig. 1.— IRTF/SpeX observations of Triton on eight consecutive nights (2002 July 15–22 UT), normalized at 1 μm and offset upward as indicated by the values in parentheses. Approximate wavelengths of various molecular absorptions are indicated along the bottom.

Fig. 2.— Enlarged view of nightly spectra of Triton's N_2 ice absorption band (gray curves), compared with the grand average (black curves).

Fig. 3.— Integrated area of Triton's N_2 ice absorption band at 2.15 μm, as a function of subsolar/sub-viewer longitude, showing a large cyclical variation. The integrated area was computed by normalizing each spectrum to a line fitted to continuum wavelengths on either side of the absorption band, then integrating one minus the normalized spectrum over the band interval. For the N_2 ice band we used 2.093 to 2.117 μm and 2.175 to 1.185 μm for the continuum and 2.117 to 2.175 μm for the band interval. Vertical error bars are formal uncertainties while horizontal bars represent the time intervals during which data were recorded. Five data points are re-plotted outside the 0° to 360° interval to clarify the periodic trend. A sinusoidal fit to the data (dotted curve) has its maximum at 19° longitude, a peak-to-peak amplitude of 96±16%, and a constant offset of 3.43×10^{-3} μm.

Fig. 4.— Numbered solid curves indicate fraction of projected full disk coverage by the six spectral units of McEwen (1990), as a function of subsolar longitude for our observing geometry. Broken lines represent sums of McEwen's units 1, 4, and 6 (the equatorial collar) and 2, 3, and 5 (the polar cap).

Fig. 5.— Integrated areas of three of Triton's CH_4 absorption band complexes, showing longitudinal trends different from that shown by the N_2 band, and also smaller fractional amplitudes. Dashed lines represent constant fits while sinusoidal fits are indicated by dotted curves with peak-to-peak amplitudes of 14±1%, 23±4%, and 65±10% from top to bottom

of the figure. For the 1.65 μm band, we used 1.605 to 1.620 μm and 1.685 to 1.699 μm for the continuum and 1.620 to 1.685 μm for the band interval. For the 1.73 μm band we used 1.686 to 1.698 μm and 1.735 to 1.745 μm for the continuum and 1.698 to 1.735 μm for the band interval. For the 0.89 μm band we used 0.860 to 0.878 μm and 0.909 to 0.930 μm for the continuum and 0.878 to 0.909 μm for the band interval.

Fig. 6.— Integrated area of Triton's 2.01 μm CO_2 absorption band, showing non-detection of any longitudinal variation. The dashed line is a constant fit and the dotted line is a sinusoidal fit with peak-to-peak amplitude 8±6%. We used 2.002 to 2.008 μm and 2.015 to 2.020 μm for the continuum and 2.008 to 2.015 μm for the band interval.

Fig. 7.— Rotational variation of the fractional band depth of Triton's 1.5 μm H_2O ice band complex, computed using the average of wavelengths from 1.500 to 1.570 μm for the band and the average of wavelengths from 1.430 to 1.450 μm and from 1.683 to 1.710 μm for the continuum. Best fit sinusoidal peak-to-peak amplitude is 35±12%.

Fig. 8.— Grand average Triton spectrum from this work (black curve) compared with Cruikshank *et al.* (2000) data (gray curve offset by +0.3). The two spectra are quite similar, but the new data have slightly higher spectral resolution, as evidenced by the narrower CO_2 bands near 2 μm.

Fig. 9.— Comparison of Triton's grand average 2.15 μm N_2 band (solid curve) with synthetic Hapke models (Hapke 1993) based on hexagonal β N_2 ice (dotted curve) and cubic α N_2 ice (dashed curve) (optical constants from Grundy *et al.* 1993). No evidence is seen for the existence of α N_2 on Triton's surface, neither at 2.148 μm nor at 2.166 μm.

Fig. 10.— Enlargement of Triton's 1.5 μm H_2O ice band complex (solid curve), compared with Hapke models (Hapke 1993) based on crystalline H_2O I_h (dotted curve) and amorphous H_2O I_a (dashed curve) optical constants from Grundy and Schmitt (1998) and Schmitt *et*

al. (1998), respectively. Crystalline H_2O ice matches Triton's H_2O ice absorption very well, while amorphous ice does not. The deep absorption bands at 1.65, 1.67, and 1.72 μm are due to CH_4 dispersed in N_2 ice, omitted from the models to show the H_2O ice absorptions more clearly.

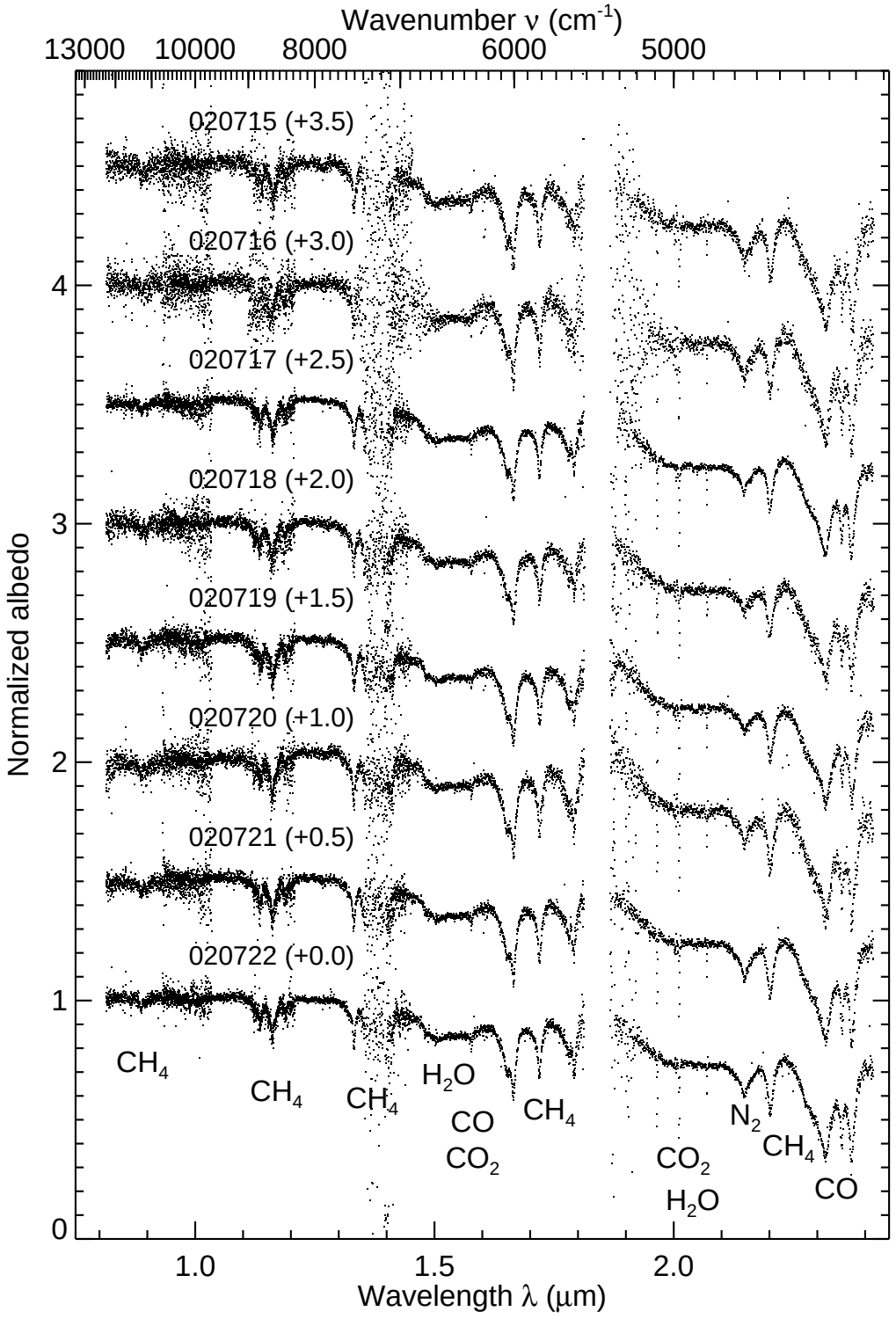

Fig. 1.— IRTF/SpeX observations of Triton on eight consecutive nights (2002 July 15–22 UT), normalized at 1 μm and offset upward as indicated by the values in parentheses. Approximate wavelengths of various molecular absorptions are indicated along the bottom.

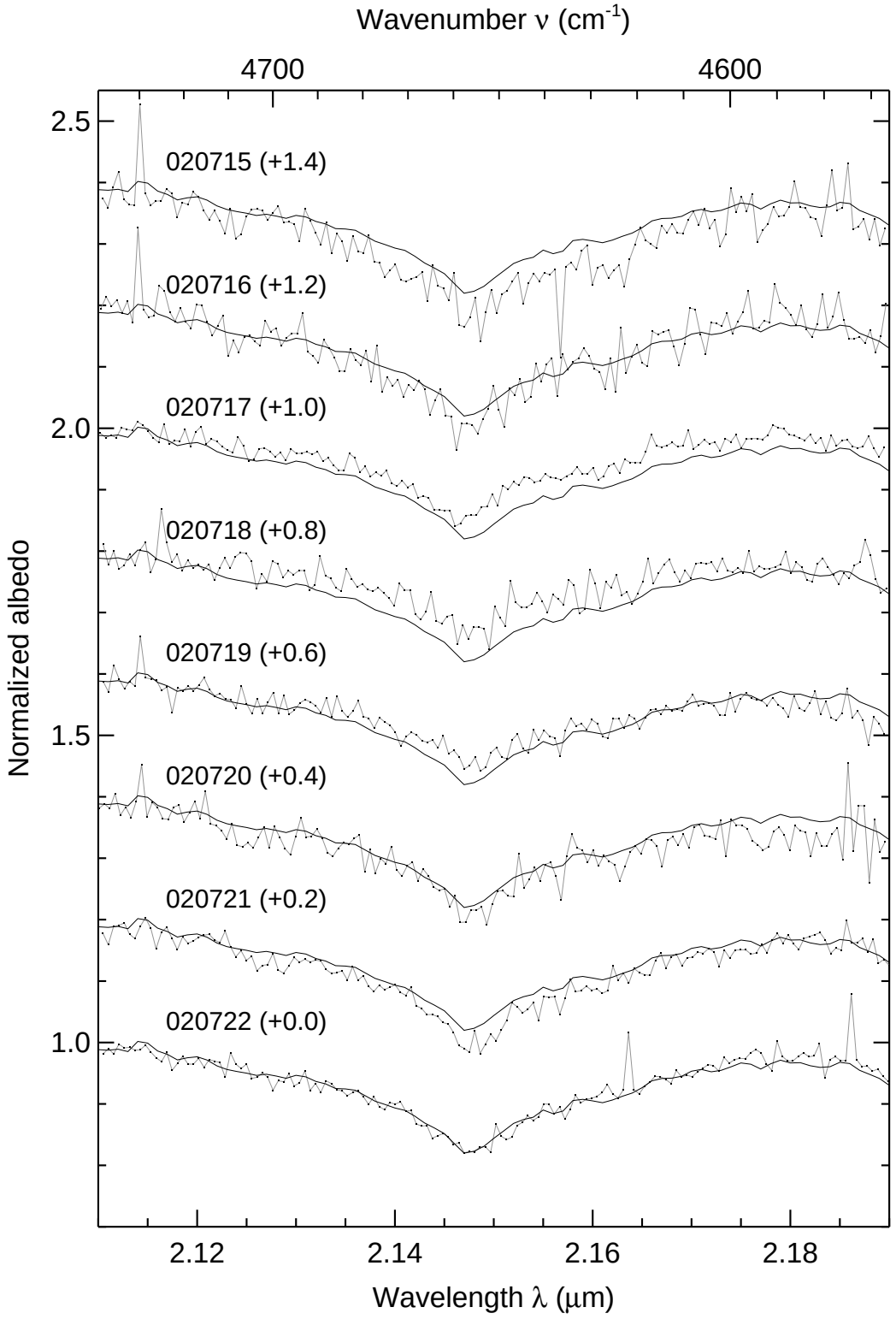

Fig. 2.— Enlarged view of nightly spectra of Triton's N_2 ice absorption band (gray curves), compared with the grand average (black curves).

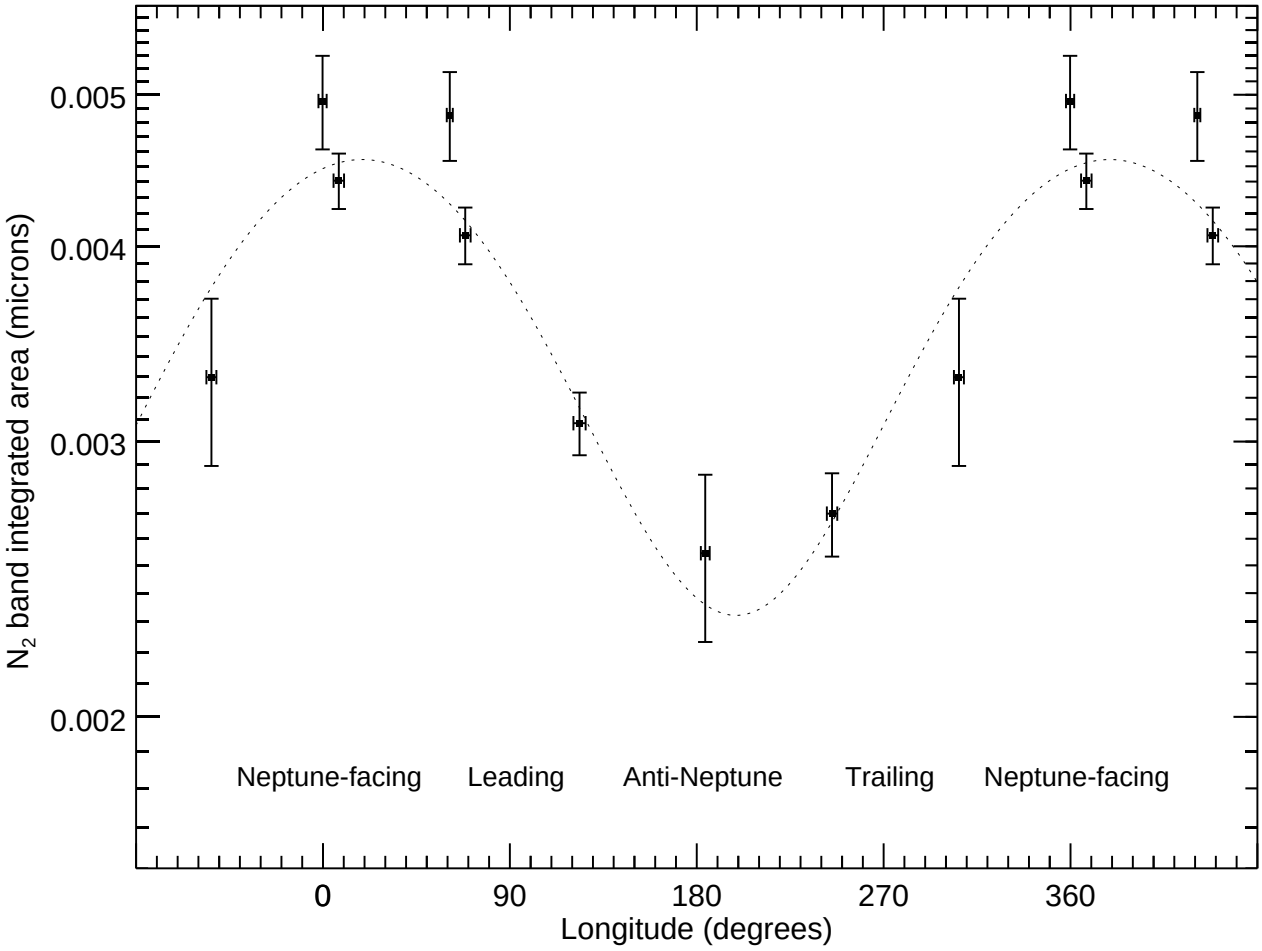

Fig. 3.— Integrated area of Triton's N_2 ice absorption band at 2.15 μm, as a function of subsolar/sub-viewer longitude, showing a large cyclical variation. The integrated area was computed by normalizing each spectrum to a line fitted to continuum wavelengths on either side of the absorption band, then integrating one minus the normalized spectrum over the band interval. For the N_2 ice band we used 2.093 to 2.117 μm and 2.175 to 1.185 μm for the continuum and 2.117 to 2.175 μm for the band interval. Vertical error bars are formal uncertainties while horizontal bars represent the time intervals during which data were recorded. Five data points are re-plotted outside the 0° to 360° interval to clarify the periodic trend. A sinusoidal fit to the data (dotted curve) has its maximum at 19° longitude, a peak-to-peak amplitude of 96±16%, and a constant offset of 3.43×10^{-3} μm.

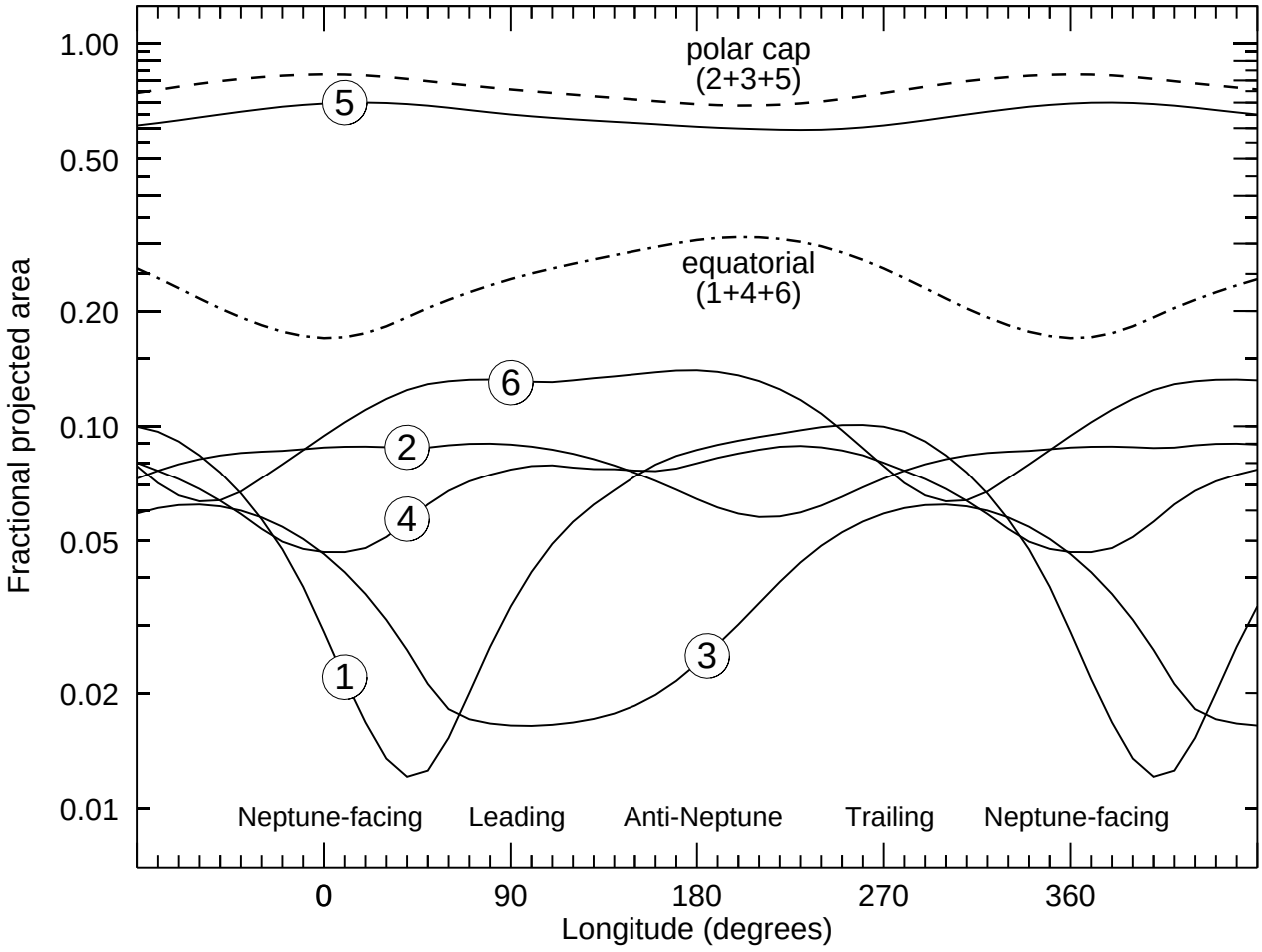

Fig. 4.— Numbered solid curves indicate fraction of projected full disk coverage by the six spectral units of McEwen (1990), as a function of subsolar longitude for our observing geometry. Broken lines represent sums of McEwen's units 1, 4, and 6 (the equatorial collar) and 2, 3, and 5 (the polar cap).

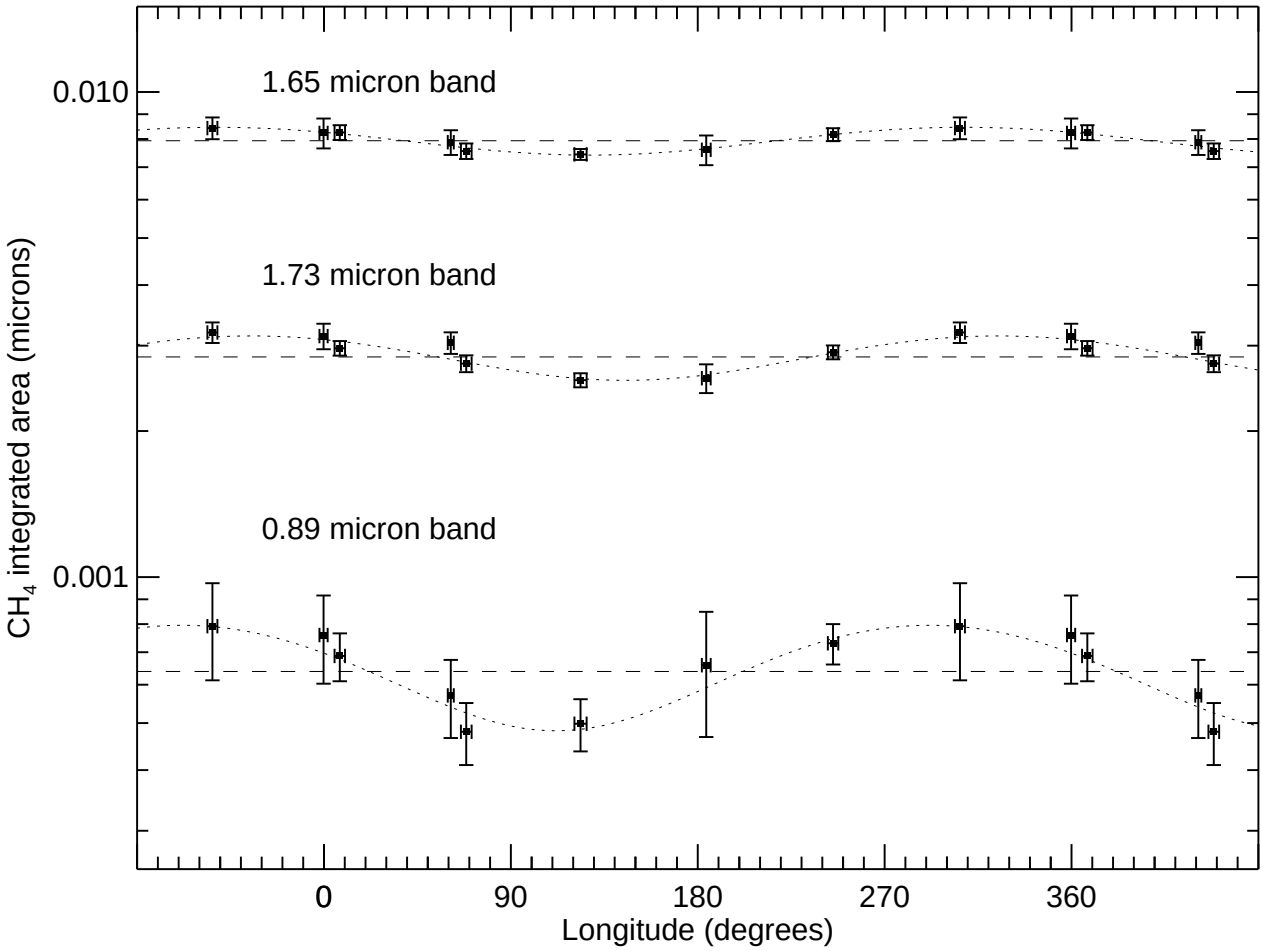

Fig. 5.— Integrated areas of three of Triton's CH_4 absorption band complexes, showing longitudinal trends different from that shown by the N_2 band, and also smaller fractional amplitudes. Dashed lines represent constant fits while sinusoidal fits are indicated by dotted curves with peak-to-peak amplitudes of 14±1%, 23±4%, and 65±10% from top to bottom of the figure. For the 1.65 μm band, we used 1.605 to 1.620 μm and 1.685 to 1.699 μm for the continuum and 1.620 to 1.685 μm for the band interval. For the 1.73 μm band we used 1.686 to 1.698 μm and 1.735 to 1.745 μm for the continuum and 1.698 to 1.735 μm for the band interval. For the 0.89 μm band we used 0.860 to 0.878 μm and 0.909 to 0.930 μm for the continuum and 0.878 to 0.909 μm for the band interval.

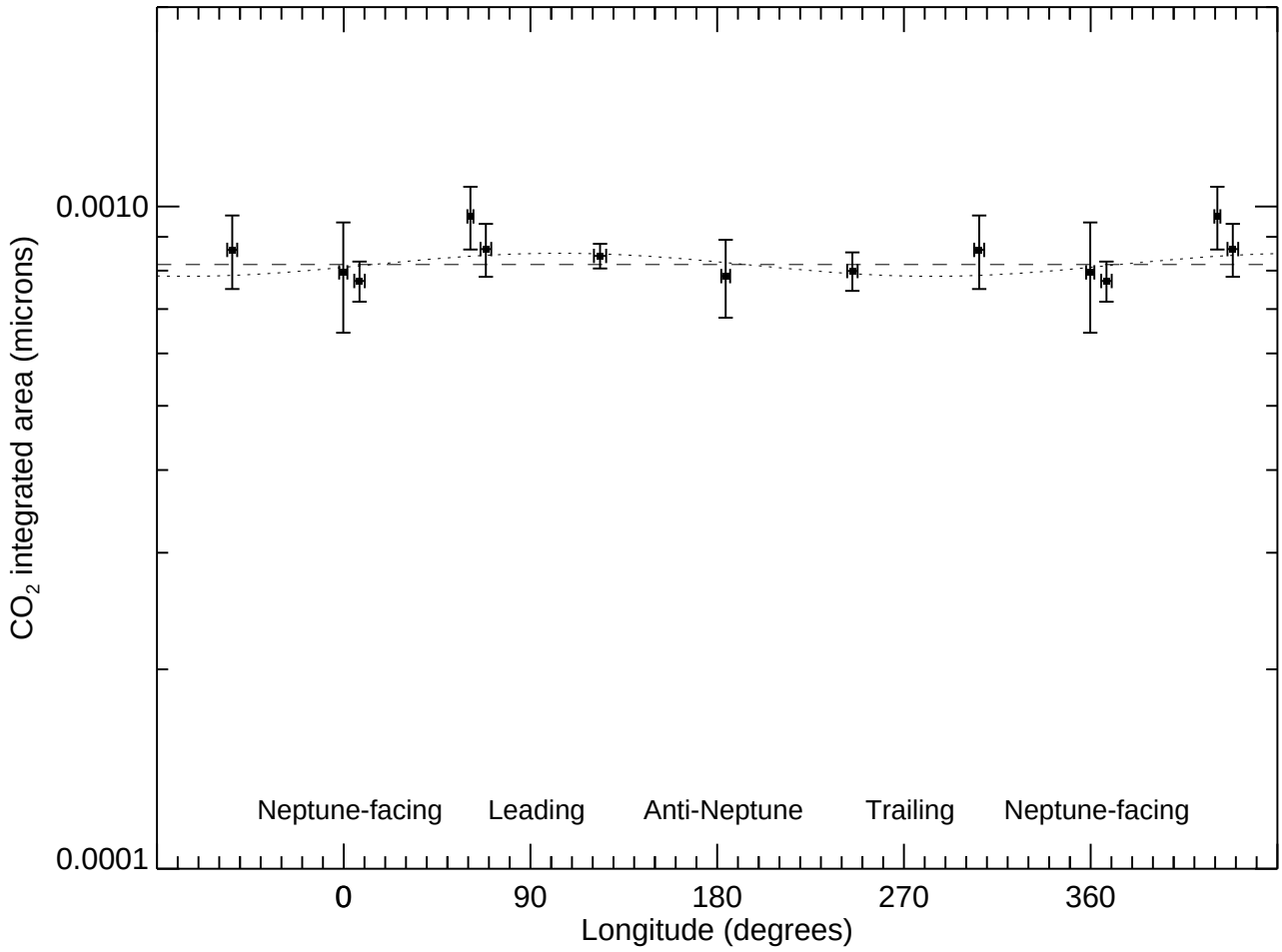

Fig. 6.— Integrated area of Triton's 2.01 μm CO_2 absorption band, showing non-detection of any longitudinal variation. The dashed line is a constant fit and the dotted line is a sinusoidal fit with peak-to-peak amplitude 8±6%. We used 2.002 to 2.008 μm and 2.015 to 2.020 μm for the continuum and 2.008 to 2.015 μm for the band interval.

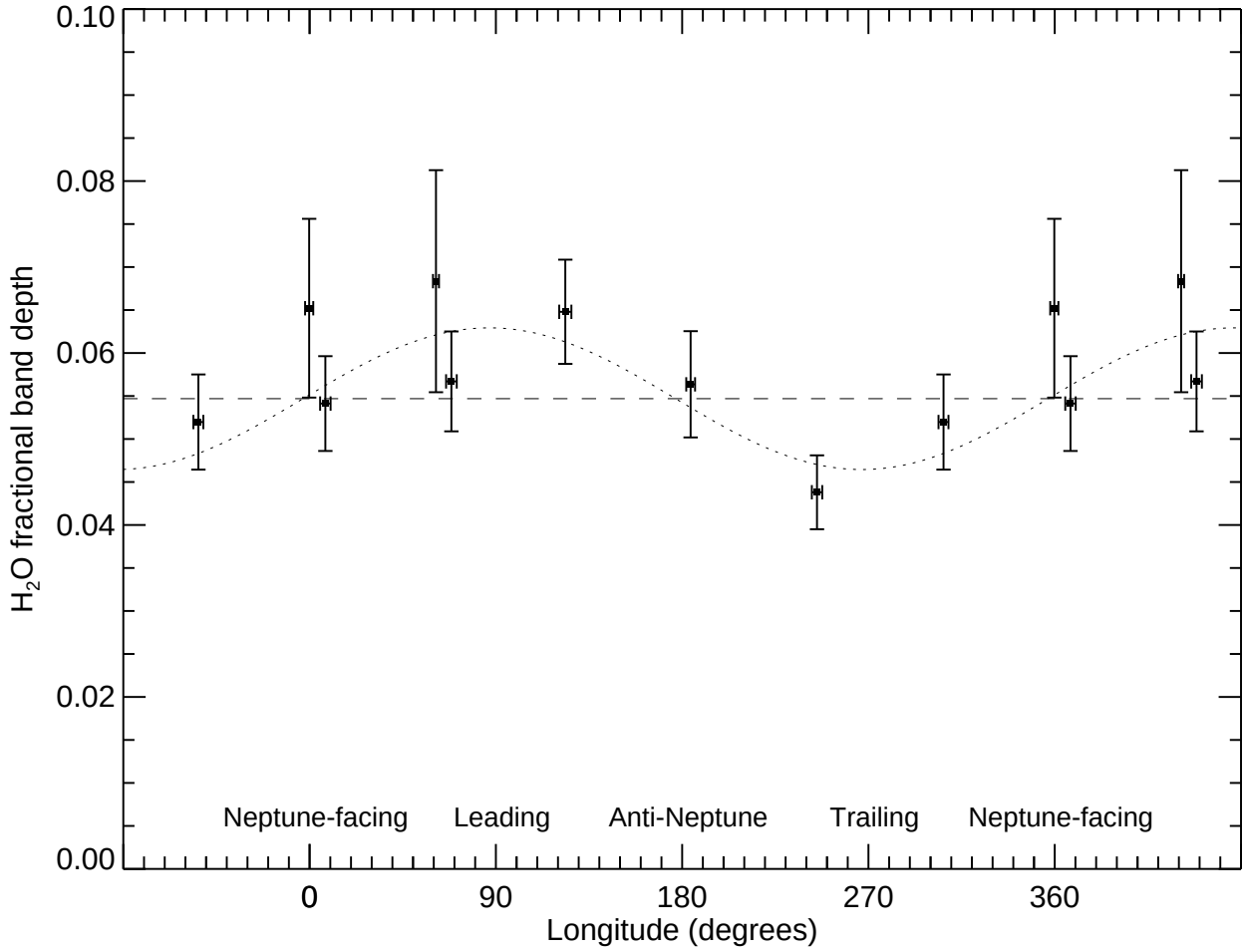

Fig. 7.— Rotational variation of the fractional band depth of Triton's 1.5 μm H_2O ice band complex, computed using the average of wavelengths from 1.500 to 1.570 μm for the band and the average of wavelengths from 1.430 to 1.450 μm and from 1.683 to 1.710 μm for the continuum. Best fit sinusoidal peak-to-peak amplitude is 35±12%.

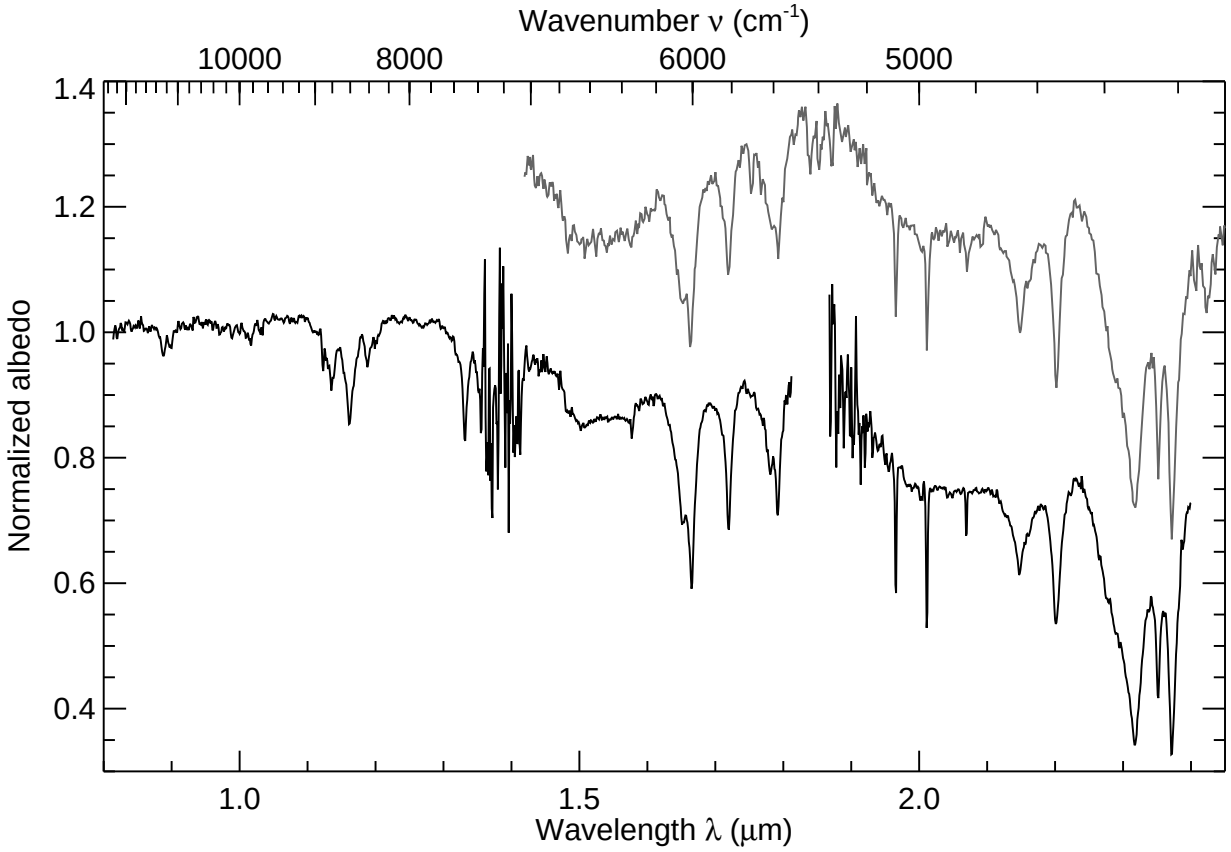

Fig. 8.— Grand average Triton spectrum from this work (black curve) compared with Cruikshank *et al.* (2000) data (gray curve offset by +0.3). The two spectra are quite similar, but the new data have slightly higher spectral resolution, as evidenced by the narrower CO_2 bands near 2 μm.

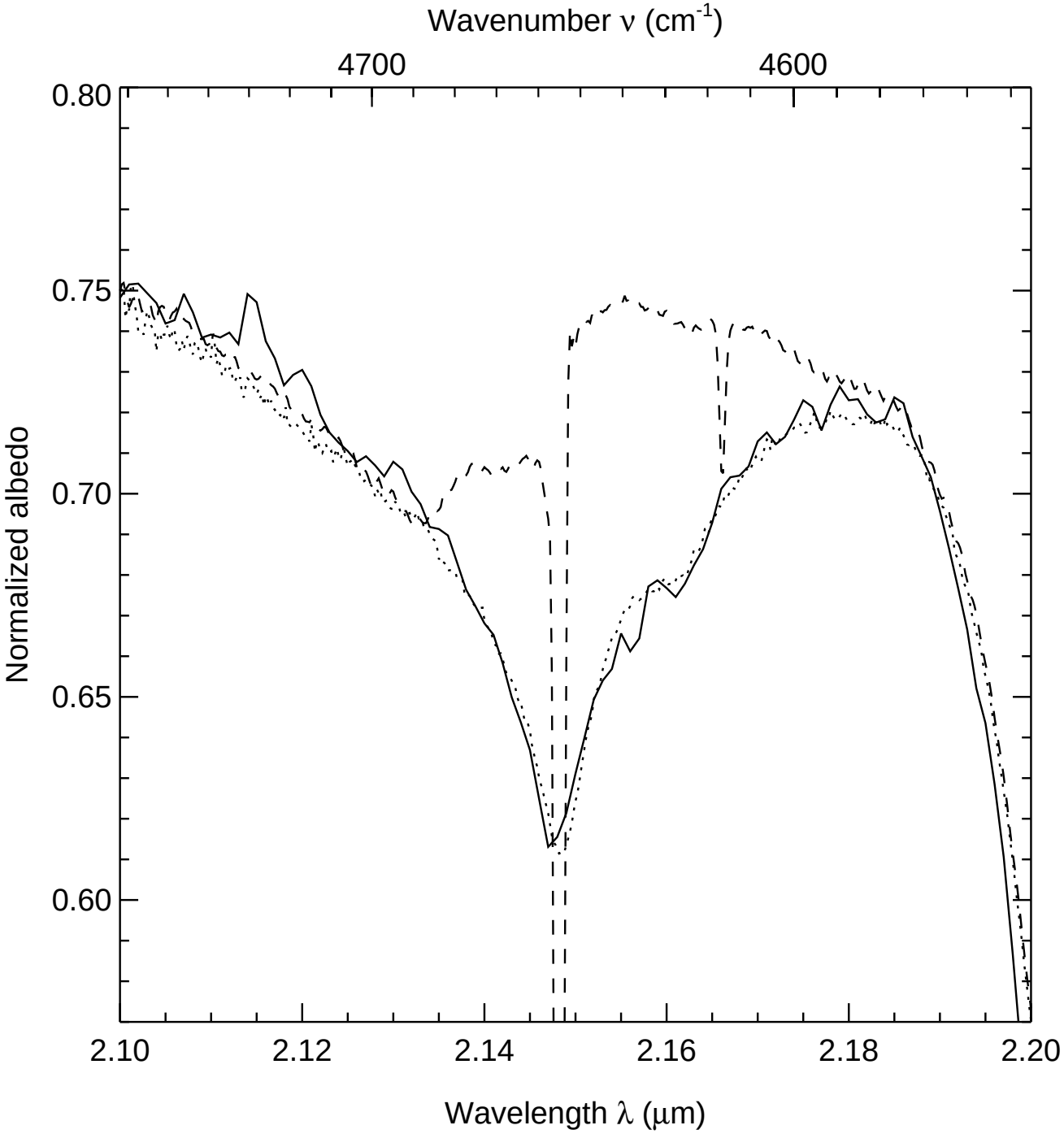

Fig. 9.— Comparison of Triton's grand average 2.15 μm N_2 band (solid curve) with synthetic Hapke models (Hapke 1993) based on hexagonal β N_2 ice (dotted curve) and cubic α N_2 ice (dashed curve) (optical constants from Grundy *et al.* 1993). No evidence is seen for the existence of α N_2 on Triton's surface, neither at 2.148 μm nor at 2.166 μm.

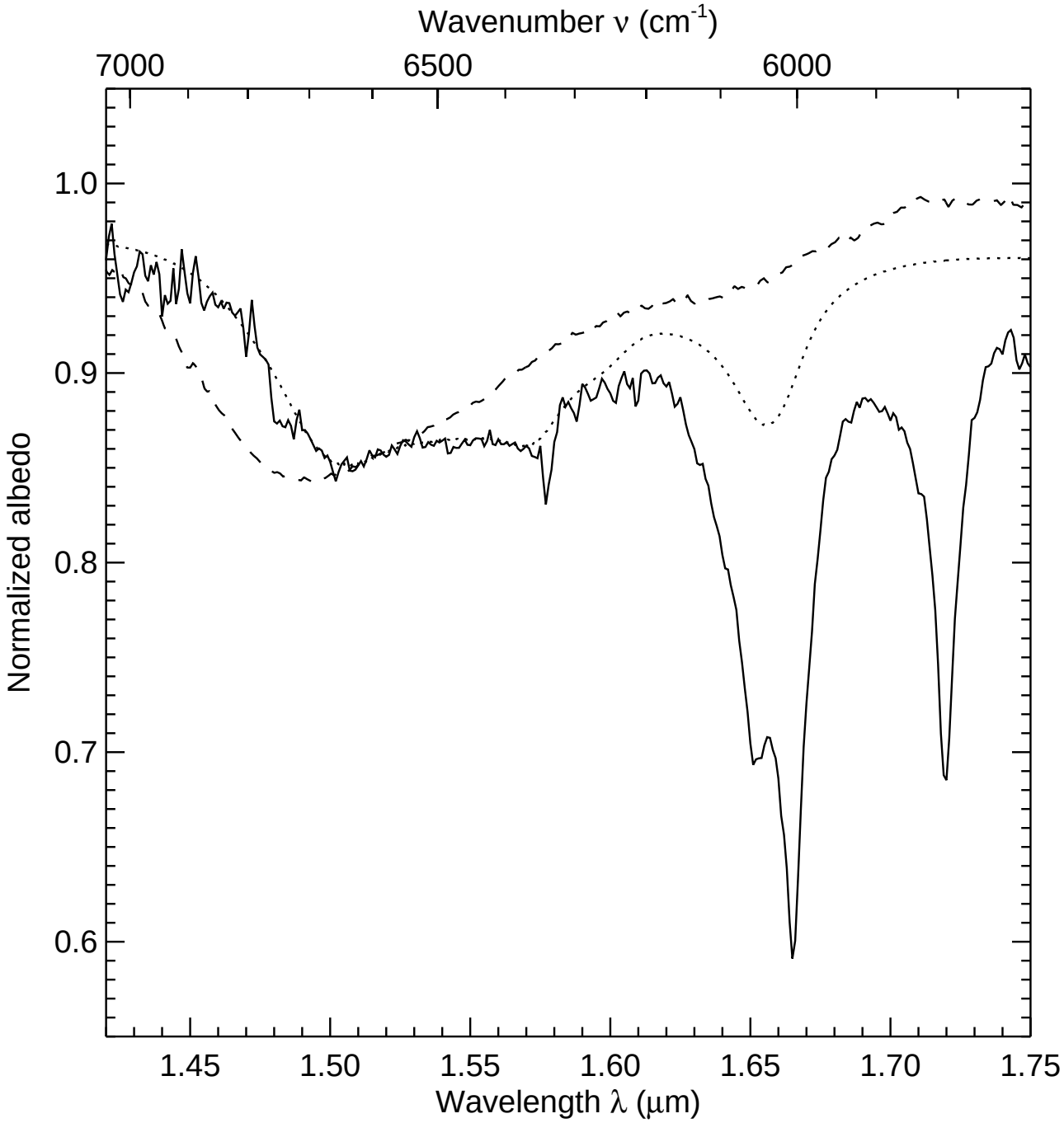

Fig. 10.— Enlargement of Triton's 1.5 μm H_2O ice band complex (solid curve), compared with Hapke models (Hapke 1993) based on crystalline H_2O I_h (dotted curve) and amorphous H_2O I_a (dashed curve) optical constants from Grundy and Schmitt (1998) and Schmitt *et al.* (1998), respectively. Crystalline H_2O ice matches Triton's H_2O ice absorption very well, while amorphous ice does not. The deep absorption bands at 1.65, 1.67, and 1.72 μm are due to CH_4 dispersed in N_2 ice, omitted from the models to show the H_2O ice absorptions more clearly.